bioRxiv preprint doi: https://doi.org/10.1101/231548; this version posted December 8, 2017. The copyright holder for this preprint (which was not certified by peer review) is the author/funder, who has granted bioRxiv a license to display the preprint in perpetuity. It is made available under aCC-BY-NC-ND 4.0 International license.

Evolution and characterization of carboplatin resistance at single cell resolution

Devora Champa[1,†], Si Sun[1,§], Cheng-Yu Tsai[1], Stephen B. Howell[1,2,*], Olivier Harismendy[1,3*]

[1]Moores UCSD Cancer Center, [2]Division of Hematology/Oncology and [3]Division of Biomedical Informatics, Department of Medicine, University of California, San Diego.

† Current address: Finnegan LLP, 3300 Hillview Ave, Palo Alto, CA

§ Current address: Department of Obstetrics and Gynecology, Union Hospital, Tongji Medical College, Huazhong University of Science and Technology, Wuhan 430022, China

• Corresponding authors: showell@ucsd.edu, oharismendy@ucsd.edu

bioRxiv preprint doi: https://doi.org/10.1101/231548; this version posted December 8, 2017. The copyright holder for this preprint (which was not certified by peer review) is the author/funder, who has granted bioRxiv a license to display the preprint in perpetuity. It is made available under aCC-BY-NC-ND 4.0 International license.

Abstract

Acquired resistance to carboplatin is a major obstacle to the cure of ovarian cancer, but its molecular underpinnings are still poorly defined. We selected multiple clones derived from a single cell in parallel for similar levels of resistance to carboplatin. The resistant clones showed no significant genetic alterations, but each one activated different mechanisms of resistance resulting in transcriptional heterogeneity. Single-cell mRNA sequencing defined multiple transcriptional states associated with clone identity and resistance evolution, and identified a subset of unselected parental cells that were already in a resistant state. Six expression signatures derived from the resistant states distinguished primary from recurrent high-grade serous ovarian cancers, predicted both response and survival and disclosed functional differences between intrinsic and acquired resistance. This multidimensional, single-cell analysis offers new insights into the dynamics of the acquisition of resistance to carboplatin, a drug of major importance to the treatment of ovarian and other cancers.

bioRxiv preprint doi: https://doi.org/10.1101/231548; this version posted December 8, 2017. The copyright holder for this preprint (which was not certified by peer review) is the author/funder, who has granted bioRxiv a license to display the preprint in perpetuity. It is made available under aCC-BY-NC-ND 4.0 International license.

Introduction

Patients diagnosed with high grade serous ovarian cancer are generally treated initially with either cisplatin or carboplatin (CBDCA) in combination with paclitaxel. While 65-75% of patients respond to the primary treatment (1), resistance emerges frequently during therapy and this is a major obstacle to cure (2). Unlike targeted agents where high-levels of resistance are common, repeated treatment of sensitive cells with clinically relevant levels of exposure to cisplatin or CBDCA produces only low-level resistance, typically in the range of 1.5-3-fold, a level sufficient to account for clinical failure of treatment *in vivo* (3).

The mechanisms underlying acquired resistance to platinum-containing drugs has been the subject of intense study ever since their discovery. Acquired resistance has been attributed to changes in many types of cellular functions including import and export of the drug, enhanced detoxification and DNA adduct repair, inactivation of the mismatch repair checkpoint and repression of apoptotic signaling (4). Findings from single genes or transcriptome-wide studies of bulk cell populations can usually be validated through overexpression or knock-out, but these studies have failed to disclose any actionable gene or set of genes that are consistently altered across different cell types or experiments and that would point toward widely useful approaches for preventing or overcoming the development of resistance in patients.

Apart from rare instances of *BRCA1/2* mutation reversion (5), the acquisition of chemo-resistance is believed to be epigenetically mediated (6). Recent advances in the study of resistance to targeted agents has revealed the existence of “persister” cells in lung cancer cell lines that are present at low prevalence and can resist treatment through epigenetic mediated mechanisms (7). Previously, single cell tracing had shown that, within a cell population, the immediate response to genotoxic treatment can vary extensively from cell to cell giving rise to considerable heterogeneity within the surviving population (8,9). More recently, similar observations were made in vemurafenib-treated melanoma cells where cells in a transient

bioRxiv preprint doi: https://doi.org/10.1101/231548; this version posted December 8, 2017. The copyright holder for this preprint (which was not certified by peer review) is the author/funder, who has granted bioRxiv a license to display the preprint in perpetuity. It is made available under aCC-BY-NC-ND 4.0 International license.

resistant state are present in the population prior to drug exposure and display increased levels of expression of resistance genes (10). Importantly, the relevance of these recent models to the acquisition of resistance to the platinum-containing drugs has not been established for either *in vitro* or *in vivo* models nor have the concepts been validated in clinical studies.

Here we present a comprehensive phenotypic and molecular characterization of a set of ovarian cancer clones derived from a single cell and selected in parallel for acquired resistance to CBDCA. We show that the resistance is unlikely to be due to genetic mutations, copy number changes or differences in CBDCA uptake. Resistance was associated with significant changes in proliferation rate and the capacity to form colonies and organoids, and there is substantial heterogeneity between clones. Transcriptome profiling showed a common association of CBDCA resistance with slow proliferation and high interferon signaling but also demonstrated marked heterogeneity between resistant clones, suggesting that the mechanisms of resistance are private to each of them. Single-cell transcriptome analysis allowed us to characterize the resistant state at single cell resolution, and to trace its evolution both during the emergence of resistance and after drug withdrawal. A gene and pathway-specific analysis further revealed the presence of small numbers of cells already in a resistant state in unselected cell populations. Importantly, the clinical expression subtypes derived from the *in vitro* resistant states associate with therapy response and outcome in patients with ovarian cancer and reveal functional differences between intrinsic and acquired resistance.

bioRxiv preprint doi: https://doi.org/10.1101/231548; this version posted December 8, 2017. The copyright holder for this preprint (which was not certified by peer review) is the author/funder, who has granted bioRxiv a license to display the preprint in perpetuity. It is made available under aCC-BY-NC-ND 4.0 International license.

Results

While resistance acquisition can be well recapitulated *in vitro*, through repeated drug exposure, variation between cell lines, methodologies and the lack of selection replicates compromise the identification of widely shared molecular changes associated with resistance to platinum-containing drugs. In order to reduce noise levels, we isolated a single cell from a non-clonal population of human ovarian cancer CAOV3 cells, and grew them to a small population (the parental clone) from which 12 clones were isolated (Figure 1A). Four of these clonal populations were grown continuously in the absence of CBDCA ("S clones": S01-S04). The remaining 8 ("R clones": R06, R07, R14-R19) were each individually subjected to 4 cycles of exposure to CBDCA at which point they tolerated 5 μM drug (subsequently referred to as step 5) and averaged 1.7-fold resistance relative to the parental clone (Figure 1B). Four of these 8 clones were then treated with additional cycles of CBDCA at gradually increasing concentrations until they tolerated 15 μM CBDCA (referred to as step 15) and averaged 7.8-fold resistance relative the parental clone. Subsequent passages of the resistant clonal populations in the absence of CBDCA for 63 doublings did not result in loss of resistance (Figure S1) indicating that the phenotype was stable after selection with high concentrations of CBDCA. This experimental design allowed us to determine, with increased confidence and rigor, whether genetically identical clones underwent the same changes during acquisition of resistance.

Phenotypic and molecular characterization of isogenic resistant clones

The phenotypic characteristics of the 4 R clones at step 15 were compared to those of the 4 S clones that had been grown continuously in the absence of drug. As shown in Figure 1C-E, the growth of the R clones was slower, they formed fewer large colonies in 2D culture, and in low-attachment plates they formed a higher proportion of tight spheres and a lower proportion of organoids. Most importantly, each of these metrics detected substantial heterogeneity among the isogenic R clones, which may be the result of small clonal differences developing during the

bioRxiv preprint doi: https://doi.org/10.1101/231548; this version posted December 8, 2017. The copyright holder for this preprint (which was not certified by peer review) is the author/funder, who has granted bioRxiv a license to display the preprint in perpetuity. It is made available under aCC-BY-NC-ND 4.0 International license.

initial round of selection or the consequences of different evolutionary trajectories during the subsequent rounds of selection.

Reduced drug uptake has been reported in many types of cells with acquired resistance to of cisplatin and CBDCA (11), but accurate measurement of initial influx rates has not been possible due to the limited sensitivity of available measurement techniques and lack of single cell resolution. Mass cytometry was used to compare cellular platinum (Pt) accumulation in the S and R clones which allowed precise quantification of Pt content in each individual cell in more than 10^5 cells per sample. After establishing the quantitative nature of this measurement (Figure S2A), we observed that the sensitive and resistant clones did not differ significantly with respect to the fraction of Pt-containing cells (Figure S2B). The total intracellular Pt content was actually slightly higher in the R than S clones ($p<0.001$, Table S1, Figure S2C,D), a change detectable only because of the ability of the mass cytometer to quantify levels in >100,000 cells per sample. However, the differences between R and S clones were very small suggesting that reduced drug uptake was not a major contributor to resistance in this model.

We sequenced the exomes of 4 S clones and 8 R clones at selection step 5 and identified a median of 39 coding mutations per clone for a total of 91 independent mutations. Sixteen mutations were non-frameshift insertions or deletions which were shared by more than 10 clones and thus less likely to be acquired in vitro, and may be due to sequencing or read alignment errors. The remaining 75 mutations affected 74 genes, 54 of which were mutated in 2 or more clones (Table S2). None of these genes were significantly more frequently mutated in the R than S clones. Similarly, we verified that the R clones did not acquire any significant shared copy number alterations when compared to the S clones (Table S3). Two clones (S01 and R06) were affected by copy number gains (4 and 10 Mbp) and 7 clones (S01-03, R06, R16, R18, R19) had copy number losses (0.2-12 M bp). When copy number changes occurred, they were small in magnitude (less than 1.5-fold) and none of them affected multiple R clones. Thus,

bioRxiv preprint doi: https://doi.org/10.1101/231548; this version posted December 8, 2017. The copyright holder for this preprint (which was not certified by peer review) is the author/funder, who has granted bioRxiv a license to display the preprint in perpetuity. It is made available under aCC-BY-NC-ND 4.0 International license.

these clonal populations derived from a single cell were genetically homogeneous and the small numbers of genetic changes observed were unlikely to be causally associated with the resistant phenotype.

In order to identify genes associated with resistance, we measured the expression level of all genes in the 4 S and the 4 R clones at step 15 using RNA-seq (Table S3). We identified 186 genes that were differentially expressed between S and R clones (Figure 2A). An enrichment analysis of Hallmark (12) and Reactome (13) gene sets revealed that resistance was associated with a global repression of proliferation and translation and the activation of genes involved with interferon signaling, *KRAS* signaling and epithelial-to-mesenchymal transition (EMT) (Figure S3). All of these are processes previously reported to be involved in chemo-resistance or response to genotoxic injury (14–16). An unsupervised analysis revealed that, while the S clones had similar transcriptional profiles, the profiles of the R clones were highly heterogeneous (Figure 2B). A clone-specific analysis showed that each R clone had deregulated different biological processes to different levels when compared to the sensitive clones (Figure 2C and Figure S4). R06 activated cell cycle and nucleotide excision repair, R14 showed the most significant EMT signature and active *KRAS* signaling, R16 had increased oxidative phosphorylation while R18 primarily activated the type I interferon response pathway. These processes are not mutually exclusive and were deregulated to different degrees in the various resistant clones. Indeed, processes related to cellular proliferation (E2F targets) were repressed in all clones, while interferon or *KRAS* signaling were induced in all clones.

Identification of resistant states at single cell resolution

Suspecting that the magnitude of the clonal heterogeneity within a cell population may be associated with the acquisition of drug resistance, especially in the initial selection phase, we measured the expression level of individual genes in ~2,000 single cells from the original CAOV3 cell population, the parental clone derived from a single cell in this population, 2 S

bioRxiv preprint doi: https://doi.org/10.1101/231548; this version posted December 8, 2017. The copyright holder for this preprint (which was not certified by peer review) is the author/funder, who has granted bioRxiv a license to display the preprint in perpetuity. It is made available under aCC-BY-NC-ND 4.0 International license.

clones and each of the 4 R clones at both selection step 5 and step 15 (Table S4). Using the expression of a median of 1,689 genes per cell, the cells were grouped by expression similarity which led to 7 major clusters referred to as cell states (Figure 3A); there was 1 large cluster (7,464 cells), 2 medium (4,028 and 6,020 cells) and 4 small (1,807-2,812 cells) clusters. The majority of cells from the original CAOV3 non-clonal population (88%), the parental clone (93%), and the S clones (91% and 97%) all resided in the largest drug sensitive state, indicating that the initial clone selection and subsequent expansion was not associated with a significant phenotypic drift (Figure 3B). Cells from the R clones at selection step 5 distributed into 2 separate states: R06 and R14 (both 94% of their cells) in one cluster and R16 and R18 (87% and 77% of their cells) in the other. Thus, at step 5, the R clones already showed divergence from the sensitive state but their relative differences were small suggesting the presence of functional similarities between them at this stage. Similar to the results from bulk RNA-seq, the R clones became very distinct after step 15 and each occupied one of 4 different more homogeneous and largely non-overlapping cell states (~88-99% of cells in each different single state).

In order to further investigate the transition between states, clone R14 was analyzed at 4 time points during the evolution of resistance: 1) at selection step 5; 2) after it became resistant to 10 μM CBDCA (step 10); 3) 40 doublings after the last 15 μM exposure to CBDCA (step 15a); and, 4) 77 doublings after the last 15 μM exposure (step 15b). After aggregating the data with those obtained from sensitive clones and the original non-clonal CAOV3 cell population, it was possible to map each time point to a different group of cells (Figure 3C). Interestingly, in this multidimensional projection, the cell clusters expanded radially as selection proceeded. Furthermore, the clusters after 40 and 77 doublings following drug removal were distinct, suggesting that the cell state continued to evolve in absence of selection, even splitting into 2 subpopulations. Such evolution was not observed in unselected cells as the parental and

bioRxiv preprint doi: https://doi.org/10.1101/231548; this version posted December 8, 2017. The copyright holder for this preprint (which was not certified by peer review) is the author/funder, who has granted bioRxiv a license to display the preprint in perpetuity. It is made available under aCC-BY-NC-ND 4.0 International license.

sensitive clones occupied the same state despite undergoing a sub-cloning step and an additional 60 doublings. This analysis clearly demonstrates that the states evolve with sequential rounds of selection and that individual clones eventually diverge into quite different states.

Characterization of resistant states at an early point during resistance evolution

In an attempt to characterize functional differences occurring early in the resistance acquisition process, we performed deeper single cell sequencing of the original CAOV3 line, the parental clone, 2 S clones and 4 step 5 resistant clones leading to reliable measurement of the expression of a larger number of genes (median: 3,636 genes/cell). At this resolution, 2 major states were identified, corresponding to sensitive and resistant cells (Figure 4A and 4B). Interestingly, while the resistant state was populated mostly with cells from resistant clones, a significant fraction of the cells from the sensitive clones were found in a resistant state including 3% from clone S02, 5% from clone S03, 7% from the parental clone and 12% from the non-clonal CAOV3 population, respectively (Figure 4B). Reciprocally, many fewer cells from the R clones were found in the sensitive state (0.7%, 0.9%, 0.6% and 3% for clone R06, R14, R16 and R18, respectively). This observation suggests that some cells within a large population of unselected cells reside in a resistant state, and that these may have a selective advantage upon exposure to the drug. Moreover, the larger fraction of cells in a resistant state found in the non-clonal CAOV3 population compared to the S02 and S03 clones indicated that resistant cells are more prevalent in the unselected population which had a higher level of clonal heterogeneity.

At the molecular level, we identified 1,289 genes with altered expression (272 upregulated, 1,017 down-regulated) in the resistant state. The two states can be distinguished by the expression level of a few processes, such as repression of cellular proliferation (E2F targets) and induction of interferon signaling (Figure 4C). These results are consistent with the findings from the bulk RNA-seq of step 15 R clones and suggest that the deregulation of these two

bioRxiv preprint doi: https://doi.org/10.1101/231548; this version posted December 8, 2017. The copyright holder for this preprint (which was not certified by peer review) is the author/funder, who has granted bioRxiv a license to display the preprint in perpetuity. It is made available under aCC-BY-NC-ND 4.0 International license.

processes, common to all R clones and associated with the step 5-resistant state, is triggered early in the resistance acquisition process. Interestingly, this single cell expression analysis not only revealed that cells from the R clones had a higher interferon signaling signature on average, but that a fraction of them were clear outliers in the distribution (Figure 4D, 1-18% with Z score>2). While such outliers are not observed in the unselected samples, the cells in a resistant state also had a higher level of interferon signaling compared to the cells in a sensitive state ($p=0.0014$) suggesting that interferon signaling contributes to the resistant state of those few cells found to be in a resistant state in the unselected population. Other processes identified in the bulk RNA-seq analysis at step 15 were not yet significantly altered at step 5 in the single cell analysis. However, individual relevant genes were overexpressed only in the R clones (Table S6 and Figure 4E-G) including those coding for vimentin, a marker of EMT transition associated with Pt drug resistance (17), *NEAT1*, a non-coding RNA regulating EMT and radio-resistance (18), and gelsolin, an apoptosis regulator previously reported to mediate resistant to the Pt drugs (19). These observations suggest that small numbers of cells already in a resistant state are important contributors to the acquisition of resistance during the selection process.

Resistant states have prognostic and functional significance for high grade serous ovarian tumors (HGSOC)

The single cell states observed at step 5 selection likely already capture the functional diversity observed between clones after step 15 selection. In addition, such processes are likely to mediate both intrinsic (in unselected cells) and acquired (in CBDCA selected cells) resistance. However, it is unknown whether these processes are active in ovarian cancers growing in patients or whether they can be used to otherwise sub-classify high-grade serous ovarian cancer (HGSOC) or predict treatment response and outcome. We used non-negative matrix factorization of the expression of 1,289 CBDCA-resistance state-defining genes in specimens from 111 HGSOC patients (20) and identified 6 transcriptional components that

bioRxiv preprint doi: https://doi.org/10.1101/231548; this version posted December 8, 2017. The copyright holder for this preprint (which was not certified by peer review) is the author/funder, who has granted bioRxiv a license to display the preprint in perpetuity. It is made available under aCC-BY-NC-ND 4.0 International license.

classified these tumors into 5 different subtypes (Figure 5A). These subtypes were named on the basis of the fraction of each tumor type or treatment response observed in a given subtype (Figure 5B). This approach identified 2 “sensitive” subtypes, A (N=12) and B (N=10), in which 79% of the tumors were sensitive. It identified a “mixed” subtype (N=21) in which 45% of the tumors were sensitive, a “resistant” subtype (N=44) in which 79% of the tumors were resistant or refractory, and a “recurrent” subtype (N=24) which contained 88% recurrent tumors. Primary tumors with a recognized homologous recombination deficiency (HRD) were more sensitive to the treatment ($p<8 \times 10^{-9}$) and, while overall they were enriched in sensitive subtypes A and B (OR=7.7, $p<8 \times 10^{-4}$), those HRD tumors that did not respond to the treatment were more likely to be in the resistant subtype (Figure 5B; OR=5.9, $p<0.017$). This suggests that the proposed sub-classification of HGSOC based on *in vitro* resistant states adds valuable information that predicts response over and above that contributed by HRD status. The 4 subtypes composed of mostly primary tumors were further associated with overall survival (log-rank p=0.004; Figure 5C), a prognostic result that was validated in HGSOC case from The Cancer Genome Atlas dataset (21) (log-rank p=0.009, Figure 5D)

Gene Set Enrichment Analysis of the subtype-defining expression components can be used to identify functional differences between HGSOC subtypes (Figure 5E). Both sensitive subtypes are characterized by cell cycle and mitotic signatures in component 2 and 3, indicative of proliferative tumors, a well-known predictor of chemo-sensitivity (22). In contrast, the resistant subtype, driven by component 1, is characterized by the absence of proliferation and enrichment of processes related to mRNA processing composed of genes encoding RNA binding proteins and forming ribonucleo-particles (ribosomes, spliceosome, RNA interference, or signal recognition particle). The mixed subtype, characterized by component 6, is similar to the resistant subtype with the addition of a high level of oxidative-phosphorylation, indicative of more metabolically active tumors. Finally, the recurrent subtype is characterized by component

bioRxiv preprint doi: https://doi.org/10.1101/231548; this version posted December 8, 2017. The copyright holder for this preprint (which was not certified by peer review) is the author/funder, who has granted bioRxiv a license to display the preprint in perpetuity. It is made available under aCC-BY-NC-ND 4.0 International license.

5 and enriched for TNFα signaling and hypoxia. Interestingly samples from recurrent tumors were primarily collected from ascites, a mostly hypoxic environment (23). Three primary tumors were also collected from ascites and displayed high level of component 5 suggesting that this functional association is driven by specimen origin rather than acquired resistance. Unlike the resistant subtype, the recurrent subtype does not show enrichment of RNA binding proteins, suggesting distinct differences between the mechanisms underlying intrinsic and acquired resistance.

bioRxiv preprint doi: https://doi.org/10.1101/231548; this version posted December 8, 2017. The copyright holder for this preprint (which was not certified by peer review) is the author/funder, who has granted bioRxiv a license to display the preprint in perpetuity. It is made available under aCC-BY-NC-ND 4.0 International license.

Discussion

In order to detect the changes that occur in human ovarian cancer cells as they become resistant to CBDCA at a high resolution, we used an isogenic system, matching resistant and sensitive samples, and multiple selection replicates. This rigorous experimental design together with the choice of the CAOV3 cell line, unambiguously originating from a patient with HGSOC (24), both contributed to reduce experimental noise relative to prior studies.

The clones' phenotypic and molecular characterization disclosed features that were shared by all R clones, distinguishing them from S clones. The R clones had lower proliferation rates, impaired ability to form colonies and organoids under low-attachment conditions, and activation of interferon signaling. Importantly, interferon signaling was already induced at step 5 selection, suggesting an early role in resistance acquisition. Activation of interferon signaling is triggered by the DNA damage response (DDR) (25) and was previously observed in response to genotoxic stress. Expression of *IRF1,* a main effector of interferon signaling*,* is induced by cisplatin and may limit this drug's effectiveness (15). Importantly, it is not yet clear whether the DDR-mediated response can be targeted to prevent or reverse resistance. In head and neck cancers, knockdown of *STAT1* reduces cell death caused by cisplatin *in vitro* (26). Similarly, silencing of *STING*, a well-known inducer of interferon, increased the efficacy of genotoxic treatment in breast cancer cell lines (27). These observations suggest that targeting interferon signaling may be a viable option to combat resistance to the Pt drugs, but such a therapeutic strategy would have to be carefully weighed against the potential anti-tumorigenic benefits of interferons (28).

While the R clones displayed common changes, they overall differed quite markedly from each other. The annotation of the expression profiles revealed that each R clone had up-regulated a different set of cellular processes suggesting that the particular combination of processes used to attain resistance was private to each clone. In contrast to prior studies which

bioRxiv preprint doi: https://doi.org/10.1101/231548; this version posted December 8, 2017. The copyright holder for this preprint (which was not certified by peer review) is the author/funder, who has granted bioRxiv a license to display the preprint in perpetuity. It is made available under aCC-BY-NC-ND 4.0 International license.

derived resistant cell lines from a heterogeneous cell population, we can confidently link the observed heterogeneity to the resistance acquisition process, as all studied clones were the progeny of a single cell and did not show any substantial genetic drift. These differences between isogenic clones may actually originate very early during the process of resistance acquisition, perhaps as soon as the first exposure to CBDCA, as has been reported for other chemotherapeutic agents when single-cell tracking assays were used (8,9).

The acquisition of resistance to CBDCA in ovarian cancer is compatible with the persister model described for resistance to *EGFR* inhibitors in several types of cancer (7,29). Cells that persist in the presence of drug concentrations that kill most of the cells in the population are characterized by low proliferation rates likely mediated by epigenetic remodeling. Similar to persister cells (30), cells with acquired resistance to CBDCA are heterogeneous, each using variable numbers of elements of a diverse set of resistance mechanisms. Since persister cells also show reduced sensitivity to cisplatin (7), it is likely that the underlying mechanisms are shared. Similar to a vemurafenib-resistant state in melanoma (10), cells in a CBDCA resistant state pre-exist in the population of parental cells. Whether this state is transient or stable is currently unknown. Interestingly, the prevalence of cells in the resistant state in the unselected population diminished with each round of sub-cloning, suggesting that genetic or epigenetic heterogeneity mediates the transition between states.

The single cell transcriptome analysis of a large number of cells in each R clone disclosed that they transited through different states as selection proceeded, and this state transition continued after the selective pressure of repeated exposure to CBDCA was stopped. This indicates that these states are not stable in culture. While the repeated cycles of CBDCA exposure likely fuels this evolution during the initial development of resistance, the selective forces operating after removal of the drug are less clear. One possibility is that cells constantly explore the state space to identify one with a faster proliferative rate. The observation that

bioRxiv preprint doi: https://doi.org/10.1101/231548; this version posted December 8, 2017. The copyright holder for this preprint (which was not certified by peer review) is the author/funder, who has granted bioRxiv a license to display the preprint in perpetuity. It is made available under aCC-BY-NC-ND 4.0 International license.

evolution continues in the absence of additional CBDCA exposure suggests the possibility that novel vulnerabilities become manifest that could be exploited to therapeutic advantage. This is a high priority topic for future investigation particularly because it may be possible to pharmacologically accelerate state transitions to re-sensitize cells.

Just as persister cells show sub-clonal heterogeneity (30), our results suggest that a population of cells in a resistant state displays substantial heterogeneity in the expression of single genes or more complex signatures. Some cells in a CBDCA-resistant state have very high levels of expression of individual genes and these cells may be those most likely to survive the next round of CBDCA exposure. Additional experiments using single cell tracking methods that can also record the level of activation of a particular resistance mechanism may be necessary to further explore the link between a transient, single-cell pre-selection resistant state and the resulting post-selection state of the population.

The expression variation between sensitive and resistant states at selection step 5 captured a large fraction of the expression variation that was highly relevant to HGSOC stratification. This is perhaps not surprising since using the expression of genes identified through the comparison of the states rather than the R and S clones is very powerful, especially given the presence of resistant cells in the untreated control population. Moreover, the vast number of cells in each state identified by single cell RNA-seq provides an unprecedented statistical power to identify significant genes that is not achievable using traditional biological replicates. Given that the genes used for the classification were derived entirely from an *in vitro* experiment, the demonstrated association between expression subtypes and primary response was surprising. This suggests that the model we used is clinically relevant, that it captures the key determinants of response, and that the contribution of factors such as grade or tumor micro-environment may already be captured by the multi-cycle, multi-replicate *in vitro* experiment carried out.

bioRxiv preprint doi: https://doi.org/10.1101/231548; this version posted December 8, 2017. The copyright holder for this preprint (which was not certified by peer review) is the author/funder, who has granted bioRxiv a license to display the preprint in perpetuity. It is made available under aCC-BY-NC-ND 4.0 International license.

The resulting tumor expression subtypes and their associated biological processes show a clear difference between cases with intrinsic versus acquired resistance. The hypoxia signature observed in recurrent tumors is likely due to the hypoxic environment of ascites (23). Hypoxia promotes chemo-resistance via pathways shared with the inflammatory response (31), but the observed molecular changes primarily expose the differences in specimen origin rather than clinical behavior. While inflammatory cytokines are present in ascites (32), our *in vitro* results suggest that the pro-inflammatory signatures can have an endogenous origin. Importantly, this inflammatory signature is only seen in recurrent tumors and not in primary tumors that do not respond, suggesting that, it is more likely to result from a recent exposure to genotoxic stress or from the ascites hypoxic environment. In contrast, intrinsic resistance in primary tumors is tightly linked to a decrease in proliferation and induction of a large set of RNA binding protein genes.

The molecular changes found in individual CBDCA-resistant clones are profoundly heterogeneous. The resistant states are plastic, changing during the course of selection and after drug exposure has been stopped. These characteristics are similar to non-genetic resistance to other chemotherapeutic agents. The development of a successful therapeutic strategy to combat and reverse chemo-resistance is therefore unlikely to result from the targeting of any one specific mechanism which may only provide a transient response. The detailed investigation of the early regulatory events underlying the emergence of resistance using single-cell tracking, expression or epigenetic profiling approaches will be critical to identify new therapeutic opportunities, optimize treatment schedule or better predict response to primary treatment.

bioRxiv preprint doi: https://doi.org/10.1101/231548; this version posted December 8, 2017. The copyright holder for this preprint (which was not certified by peer review) is the author/funder, who has granted bioRxiv a license to display the preprint in perpetuity. It is made available under aCC-BY-NC-ND 4.0 International license.

Materials and Methods

Generation of CBDCA resistant clones

CAOV3 cells and all sublines were grown in RPMI 1640 containing 5% fetal bovine serum and 1X penicillin/streptomycin. The clonally derived cell lines were always plated at 40,000 cells per well in 6 well plates and allowed to attach overnight before adding the drug. A selection cycle consisted of exposure to the drug for 7 days following which cells were allowed to recover in drug-free medium for ~2 weeks until they resumed growth and reached confluence. CBDCA sensitivity was determined from concentration-survival curves using ≥5 concentrations; viability was determined with the Cell Counting Kit 8 (Dojindo Molecular Technologies, Rockville, MD) or Crystal Violet reagent after 96 h of drug exposure.

2D and 3D Growth Assays

CAOV3 cells were seeded at 200 cells/well in a 6-well plate in replicates of 3 or 6 and allowed to form colonies for 9 days after which they were stained with Crystal Violet. Colonies were counted microscopically. The capacity to grow in 3 dimensions was tested by seeding 20,000 cells/well in ultra-low attachment 6 well plates (Corning Ref 3471) in stem cell medium (1:1 DMEM:F12 plus L-glutamine, 15 mM HEPES, 100 U/mL penicillin, 100 µg/mL streptomycin, 1% knockout serum replacement, 0.4% bovine serum albumin, and 0.1% insulin-transferrin-selenium (Corning, Corning, NY). The stem cell medium was further supplemented with human recombinant epidermal growth factor (20 ng/mL) and human recombinant basic fibroblast growth factor (10 ng/mL). The medium in each well was refreshed every 3 days by adding 500 µL/well of fresh stem cell media supplemented with the growth factors. Spheres were counted under a microscope and subclassified as either tight spheres or organoids after 7 and 14 days of culture.

Mass Cytometry

bioRxiv preprint doi: https://doi.org/10.1101/231548; this version posted December 8, 2017. The copyright holder for this preprint (which was not certified by peer review) is the author/funder, who has granted bioRxiv a license to display the preprint in perpetuity. It is made available under aCC-BY-NC-ND 4.0 International license.

Cells were incubated with 15 μM CBDCA for 1 h at 37°C, washed and then exposed to a 1:500 dilution of Cell-ID Intercalator ^{103}Rh for 15 min at 37°C to mark the dead cells in the population. Analysis of ~2 x10^5 cells from each sample was carried out on a Fluidigm Helios mass cytometer using EQ Four Element Calibration Beads for normalization.

Exome Sequencing and Analysis

The sequencing libraries were prepared and captured using SureSelect Human All Exon V4 kit (Agilent Technologies) following the manufacturer's instructions. The sequencing was performed using the Illumina HiSeq 2000 system, generating 100 bp paired-end reads. All raw 100 bp paired-end reads were aligned to the human genome reference sequence (hg19) using BWA (33) and further jointly realigned around indels sites using GATK's (34) IndelRealigner. Duplicate reads were removed using Picard Tools MarkDuplicates (35). Table S6 presents the summary statistics of the sequencing. The variants were called using Freebayes (36) and filtered for high quality (QUAL/AO>10). We annotated the variants with ANNOVAR (37), removed non-coding and synonymous variants, variants in dbSNP147 or shared between all samples, leading to a total of 93 variants across all 8 samples (Table S2). The copy number changes were called independently on each chromosome using CODEX (38) with default settings (Table S3), limited to the expected exonic target from the SureSelect capture kits and expecting fractional copy number from aneuploidy. Segments smaller than 100kb, supported by less than 3 exons, or with copy number between 1.5 and 2.5 were excluded.

RNA Sequencing and Analysis

RNA was extracted using Qiagen RNAEasy and the libraries were prepared from 1 μg of RNA using TruSeq following the manufacturer instructions (shear time modified to 5 min). The libraries were sequenced on HiSeq 4000 (paired end 100 nt reads) and analyzed using BCBio-nextgen 1.0.1 (39) RNA-Seq default pipeline which included adapter removal with cutadapt v1.12 (40), read splice aware alignment with Bowtie2/Tophat suite v2.22.8 (41,42) for quality

bioRxiv preprint doi: https://doi.org/10.1101/231548; this version posted December 8, 2017. The copyright holder for this preprint (which was not certified by peer review) is the author/funder, who has granted bioRxiv a license to display the preprint in perpetuity. It is made available under aCC-BY-NC-ND 4.0 International license.

control (Table S7), and isoform expression level estimation using sailfish 0.10.1 (43). The differential expression was determined using DESeq2 (44). We performed Gene Set Enrichment Analysis (45) using gene set from MSigDB (46) and implemented in the *liger* R package.

Single cell RNA-Sequencing

We used the 10x Chromium (10x Genomics v2 reagents) to isolate ~2000 single cells from each sample following the manufacturer's instructions. Briefly the cells/GEM droplets emulsion was formed using 10x Chromium controller. The reverse transcription and template switching steps added both a cell-specific barcode and unique molecular identifier to each cDNA. The emulsion was then broken up and the GEM cleaned up. The single-strand cDNA was fragmented enzymatically and subjected to library preparation, including clean-up, end-repair, adapter ligation and enrichment PCR to add sample-specific index. The libraries were quantified using Agilent Tape-station, and pooled for sequencing on the Illumina HiSeq 4000 for single index paired-end sequencing (28+98nt reads). The resulting sequencing reads were separated using bcl2fastq and analyzed using the Cell Ranger v2 pipeline *count*, combining reads from different sequencing runs. The barcode/cell matrices from different samples were further aggregated using Cell Ranger *aggregate* normalizing to total number of reads (Table S4). The resulting multi-sample cell/barcode matrix was then analyzed using cellRangerkit R package. Notably, each sample was sequenced at different depth, thus requiring down-sampling the reads before aggregation. This led us to three sample aggregation schemes (Table S4): 1) *broad*: includes all unselected, step 5 and step 15 selected samples (median of 15,981 reads per cell), 2) *deep*: includes unselected and step 5 selected samples (median 41,523 reads per cell), 3) *R14 focused*: includes unselected and all R14 selected samples (median 14,731 reads per cell). We used a graph-based clustering default settings from CellRanger and adapted from Macosko et al (47). The clusters were further consolidated according to their distribution in the tSNE projection. Differentially expressed genes were identified using the Cell Ranger

bioRxiv preprint doi: https://doi.org/10.1101/231548; this version posted December 8, 2017. The copyright holder for this preprint (which was not certified by peer review) is the author/funder, who has granted bioRxiv a license to display the preprint in perpetuity. It is made available under aCC-BY-NC-ND 4.0 International license.

implementation of *sseq* (48). The pathway score for each cell was determined using the bioconductor *gsva* package.

Clinical sample classification and prognosis

The gene expression from the ICGC high grade serous ovarian cancer (20) was obtained directly from the ICGC portal (49). The expression level was available for 1251/1289 genes, rescaled (z-score transform), outliers were collapsed to a maximum of 3 standard deviation and all scores were made positive (adding 3). The rank of the non-negative matrix factorization was identified using *Findrank* of the *NMF* R package, and the matrix was decomposed at the chosen rank (k=6) using 100 permutations. The samples were clustered according to the resulting component level using *pheatmap* and *cutree* packages. The gene expression data from TCGA (21) was obtained from the Broad institute *Firehose* API (RSEM normalized, v2016012800) and scaled the same way. The subtype membership of each sample was determined as the subtype with maximal Pearson correlation (greater than 0.2) to each cluster-specific meta-gene expression derived from ICGC data. Survival analysis were performed using R package 'survival' and significance determined using log-rank test.

bioRxiv preprint doi: https://doi.org/10.1101/231548; this version posted December 8, 2017. The copyright holder for this preprint (which was not certified by peer review) is the author/funder, who has granted bioRxiv a license to display the preprint in perpetuity. It is made available under aCC-BY-NC-ND 4.0 International license.

Acknowledgements

We thank Drs. Pablo Tamayo and Jack Bui for helpful discussions. We thank Mr. Gerald Manorek for technical assistance as well as Dr. Lyn Hedrick and Erik Ehinger for assistance with the Mass cytometry assays. The work was funded by grants from the National Cancer Institute (R21CA177519), from the Department of Defense (OC140179), an award from Pedal the Cause and a grant from the UC San Diego Academic Senate.

Data availability

The data generated are available at the NCBI under bioproject PRJNA419934

bioRxiv preprint doi: https://doi.org/10.1101/231548; this version posted December 8, 2017. The copyright holder for this preprint (which was not certified by peer review) is the author/funder, who has granted bioRxiv a license to display the preprint in perpetuity. It is made available under aCC-BY-NC-ND 4.0 International license.

References

1. Ozols RF, Bundy BN, Greer BE, Fowler JM, Clarke-Pearson D, Burger RA, et al. Phase III trial of carboplatin and paclitaxel compared with cisplatin and paclitaxel in patients with optimally resected stage III ovarian cancer: a Gynecologic Oncology Group study. J Clin Oncol. 2003;21:3194–200.

2. Siegel R, Naishadham D, Jemal A. Cancer statistics, 2013. CA Cancer J Clin. 2013;63:11–30.

3. Andrews PA, Jones JA, Varki NM, Howell SB. Rapid emergence of acquired cis-diamminedichloroplatinum(II) resistance in an in vivo model of human ovarian carcinoma. Cancer Commun. 1990;2:93–100.

4. Galluzzi L, Senovilla L, Vitale I, Michels J, Martins I, Kepp O, et al. Molecular mechanisms of cisplatin resistance. Oncogene. 2012;31:1869–83.

5. Sakai W, Swisher EM, Karlan BY, Agarwal MK, Higgins J, Friedman C, et al. Secondary mutations as a mechanism of cisplatin resistance in BRCA2-mutated cancers. Nature. 2008;451:1116–20.

6. Brown R, Curry E, Magnani L, Wilhelm-Benartzi CS, Borley J. Poised epigenetic states and acquired drug resistance in cancer. Nat Rev Cancer. 2014;14:747–53.

7. Sharma S V, Lee DY, Li B, Quinlan MP, Takahashi F, Maheswaran S, et al. A chromatin-mediated reversible drug-tolerant state in cancer cell subpopulations. Cell. 2010;141:69–80.

8. Gascoigne KE, Taylor SS. Cancer Cells Display Profound Intra- and Interline Variation following Prolonged Exposure to Antimitotic Drugs. Cancer Cell. 2008;14:111–22.

9. Cohen AA, Geva-Zatorsky N, Eden E, Frenkel-Morgenstern M, Issaeva I, Sigal A, et al.

bioRxiv preprint doi: https://doi.org/10.1101/231548; this version posted December 8, 2017. The copyright holder for this preprint (which was not certified by peer review) is the author/funder, who has granted bioRxiv a license to display the preprint in perpetuity. It is made available under aCC-BY-NC-ND 4.0 International license.

Dynamic Proteomics of Individual Cancer Cells in Response to a Drug. Science (80-). 2008;322:1511–6.

10. Shaffer SM, Dunagin MC, Torborg SR, Torre EA, Emert B, Krepler C, et al. Rare cell variability and drug-induced reprogramming as a mode of cancer drug resistance. Nature. 2017;546:431–5.

11. Abada P, Howell SB. Regulation of Cisplatin cytotoxicity by cu influx transporters. Met Based Drugs. 2010;2010:317581.

12. Liberzon A, Birger C, Thorvaldsdottir H, Ghandi M, Mesirov JP, Tamayo P. The Molecular Signatures Database (MSigDB) hallmark gene set collection. Cell Syst. 2015;1:417–25.

13. Fabregat A, Jupe S, Matthews L, Sidiropoulos K, Gillespie M, Garapati P, et al. The Reactome Pathway Knowledgebase. Nucleic Acids Res. 2017;

14. Brzostek-Racine S, Gordon C, Van Scoy S, Reich NC. The DNA Damage Response Induces IFN. J Immunol. 2011;187:5336–45.

15. Pavan S, Olivero M, Corà D, Di Renzo MF. IRF-1 expression is induced by cisplatin in ovarian cancer cells and limits drug effectiveness. Eur J Cancer. 2013;49:964–73.

16. Yang AD, Fan F, Camp ER, van Buren G, Liu W, Somcio R, et al. Chronic Oxaliplatin Resistance Induces Epithelial-to-Mesenchymal Transition in Colorectal Cancer Cell Lines. Clin Cancer Res. 2006;12:4147 LP-4153.

17. Haslehurst AM, Koti M, Dharsee M, Nuin P, Evans K, Geraci J, et al. EMT transcription factors snail and slug directly contribute to cisplatin resistance in ovarian cancer. BMC Cancer. 2012;12:91.

18. Lu Y, Li T, Wei G, Liu L, Chen Q, Xu L, et al. The long non-coding RNA NEAT1 regulates epithelial to mesenchymal transition and radioresistance in through miR-204/ZEB1 axis in

bioRxiv preprint doi: https://doi.org/10.1101/231548; this version posted December 8, 2017. The copyright holder for this preprint (which was not certified by peer review) is the author/funder, who has granted bioRxiv a license to display the preprint in perpetuity. It is made available under aCC-BY-NC-ND 4.0 International license.

nasopharyngeal carcinoma. Tumor Biol. 2016;37:11733–41.

19. Abedini MR, Wang P-W, Huang Y-F, Cao M, Chou C-Y, Shieh D-B, et al. Cell fate regulation by gelsolin in human gynecologic cancers. Proc Natl Acad Sci . 2014;111:14442–7.

20. Patch A-M, Christie EL, Etemadmoghadam D, Garsed DW, George J, Fereday S, et al. Whole–genome characterization of chemoresistant ovarian cancer. Nature. 2015;521:489–94.

21. Integrated genomic analyses of ovarian carcinoma. Nature. 2011;474:609–15.

22. Jazaeri AA, Awtrey CS, Chandramouli GVR, Chuang YE, Khan J, Sotiriou C, et al. Gene expression profiles associated with response to chemotherapy in epithelial ovarian cancers. Clin Cancer Res. 2005;11:6300–10.

23. Kim K-S, Sengupta S, Berk M, Kwak Y-G, Escobar PF, Belinson J, et al. Hypoxia enhances lysophosphatidic acid responsiveness in ovarian cancer cells and lysophosphatidic acid induces ovarian tumor metastasis in vivo. Cancer Res. 2006;66:7983–90.

24. Beaufort CM, Helmijr JCA, Piskorz AM, Hoogstraat M, Ruigrok-Ritstier K, Besselink N, et al. Ovarian cancer cell line panel (OCCP): clinical importance of in vitro morphological subtypes. PLoS One. 2014;9:e103988.

25. Nakad R, Schumacher B. DNA Damage Response and Immune Defense: Links and Mechanisms. Front Genet. 2016;7:147.

26. Schmitt NC, Trivedi S, Ferris RL. STAT1 Activation Is Enhanced by Cisplatin and Variably Affected by EGFR Inhibition in HNSCC Cells. Mol Cancer Ther. 2015;14:2103–11.

27. Gaston J, Cheradame L, Yvonnet V, Deas O, Poupon M-F, Judde J-G, et al. Intracellular

bioRxiv preprint doi: https://doi.org/10.1101/231548; this version posted December 8, 2017. The copyright holder for this preprint (which was not certified by peer review) is the author/funder, who has granted bioRxiv a license to display the preprint in perpetuity. It is made available under aCC-BY-NC-ND 4.0 International license.

STING inactivation sensitizes breast cancer cells to genotoxic agents. Oncotarget. 2016;7:77205–24.

28. Parker BS, Rautela J, Hertzog PJ. Antitumour actions of interferons: implications for cancer therapy. Nat Rev Cancer. 2016;16:131–44.

29. Hangauer MJ, Viswanathan VS, Ryan MJ, Bole D, Eaton JK, Matov A, et al. Drug-tolerant persister cancer cells are vulnerable to GPX4 inhibition. Nature. 2017;551:247–50.

30. Ramirez M, Rajaram S, Steininger RJ, Osipchuk D, Roth MA, Morinishi LS, et al. Diverse drug-resistance mechanisms can emerge from drug-tolerant cancer persister cells. Nat Commun. 2016;7:10690.

31. Selvendiran K, Bratasz A, Kuppusamy ML, Tazi MF, Rivera BK, Kuppusamy P. Hypoxia induces chemoresistance in ovarian cancer cells by activation of signal transducer and activator of transcription 3. Int J cancer. 2009;125:2198–204.

32. Matte I, Lane D, Laplante C, Rancourt C, Piche A. Profiling of cytokines in human epithelial ovarian cancer ascites. Am J Cancer Res. 2012;2:566–80.

33. Li H, Durbin R. Fast and accurate short read alignment with Burrows-Wheeler transform. Bioinformatics. 2009/05/20. 2009;25:1754–60.

34. McKenna A, Hanna M, Banks E, Sivachenko A, Cibulskis K, Kernytsky A, et al. The Genome Analysis Toolkit: a MapReduce framework for analyzing next-generation DNA sequencing data. Genome Res. 2010/07/21. 2010;20:1297–303.

35. Picard [Internet]. Available from: http://sourceforge.net/projects/picard/

36. Garrison E, Marth G. Haplotype-based variant detection from short-read sequencing. 2012;9.

37. Wang K, Li M, Hakonarson H. ANNOVAR: functional annotation of genetic variants from

bioRxiv preprint doi: https://doi.org/10.1101/231548; this version posted December 8, 2017. The copyright holder for this preprint (which was not certified by peer review) is the author/funder, who has granted bioRxiv a license to display the preprint in perpetuity. It is made available under aCC-BY-NC-ND 4.0 International license.

high-throughput sequencing data. Nucleic Acids Res. 2010;38:e164.

38. Jiang Y, Oldridge DA, Diskin SJ, Zhang NR. CODEX: a normalization and copy number variation detection method for whole exome sequencing. Nucleic Acids Res. 2015;43:e39.

39. bcbio-nextgen [Internet]. Available from: https://github.com/chapmanb/bcbio-nextgen

40. Martin M. Cutadapt removes adapter sequences from high-throughput sequencing reads. EMBnet.journal; Vol 17, No 1 Next Gener Seq Data Anal. 2011;

41. Langmead B, Salzberg SL. Fast gapped-read alignment with Bowtie 2. Nat Meth. 2012;advance on.

42. Kim D, Pertea G, Trapnell C, Pimentel H, Kelley R, Salzberg S. TopHat2: accurate alignment of transcriptomes in the presence of insertions, deletions and gene fusions. Genome Biol. 2013;14:R36.

43. Patro R, Mount SM, Kingsford C. Sailfish enables alignment-free isoform quantification from RNA-seq reads using lightweight algorithms. Nat Biotechnol. 2014;32:462–4.

44. Love MI, Huber W, Anders S. Moderated estimation of fold change and dispersion for RNA-seq data with DESeq2. Genome Biol. 2014;15:550.

45. Subramanian A, Tamayo P, Mootha VK, Mukherjee S, Ebert BL, Gillette MA, et al. Gene set enrichment analysis: a knowledge-based approach for interpreting genome-wide expression profiles. Proc Natl Acad Sci U S A. 2005;102:15545–50.

46. Liberzon A, Subramanian A, Pinchback R, Thorvaldsdóttir H, Tamayo P, Mesirov JP. Molecular Signatures Database (MSigDB) 3.0. Bioinformatics. 2011;

47. Macosko EZ, Basu A, Satija R, Nemesh J, Shekhar K, Goldman M, et al. Highly Parallel Genome-wide Expression Profiling of Individual Cells Using Nanoliter Droplets. Cell.

bioRxiv preprint doi: https://doi.org/10.1101/231548; this version posted December 8, 2017. The copyright holder for this preprint (which was not certified by peer review) is the author/funder, who has granted bioRxiv a license to display the preprint in perpetuity. It is made available under aCC-BY-NC-ND 4.0 International license.

2017;161:1202–14.

48. Yu D, Huber W, Vitek O. Shrinkage estimation of dispersion in Negative Binomial models for RNA-seq experiments with small sample size. Bioinformatics. 2013;29:1275–82.

49. Zhang J, Baran J, Cros A, Guberman JM, Haider S, Hsu J, et al. International Cancer Genome Consortium Data Portal--a one-stop shop for cancer genomics data. Database (Oxford). 2011;2011:bar026.

bioRxiv preprint doi: https://doi.org/10.1101/231548; this version posted December 8, 2017. The copyright holder for this preprint (which was not certified by peer review) is the author/funder, who has granted bioRxiv a license to display the preprint in perpetuity. It is made available under aCC-BY-NC-ND 4.0 International license.

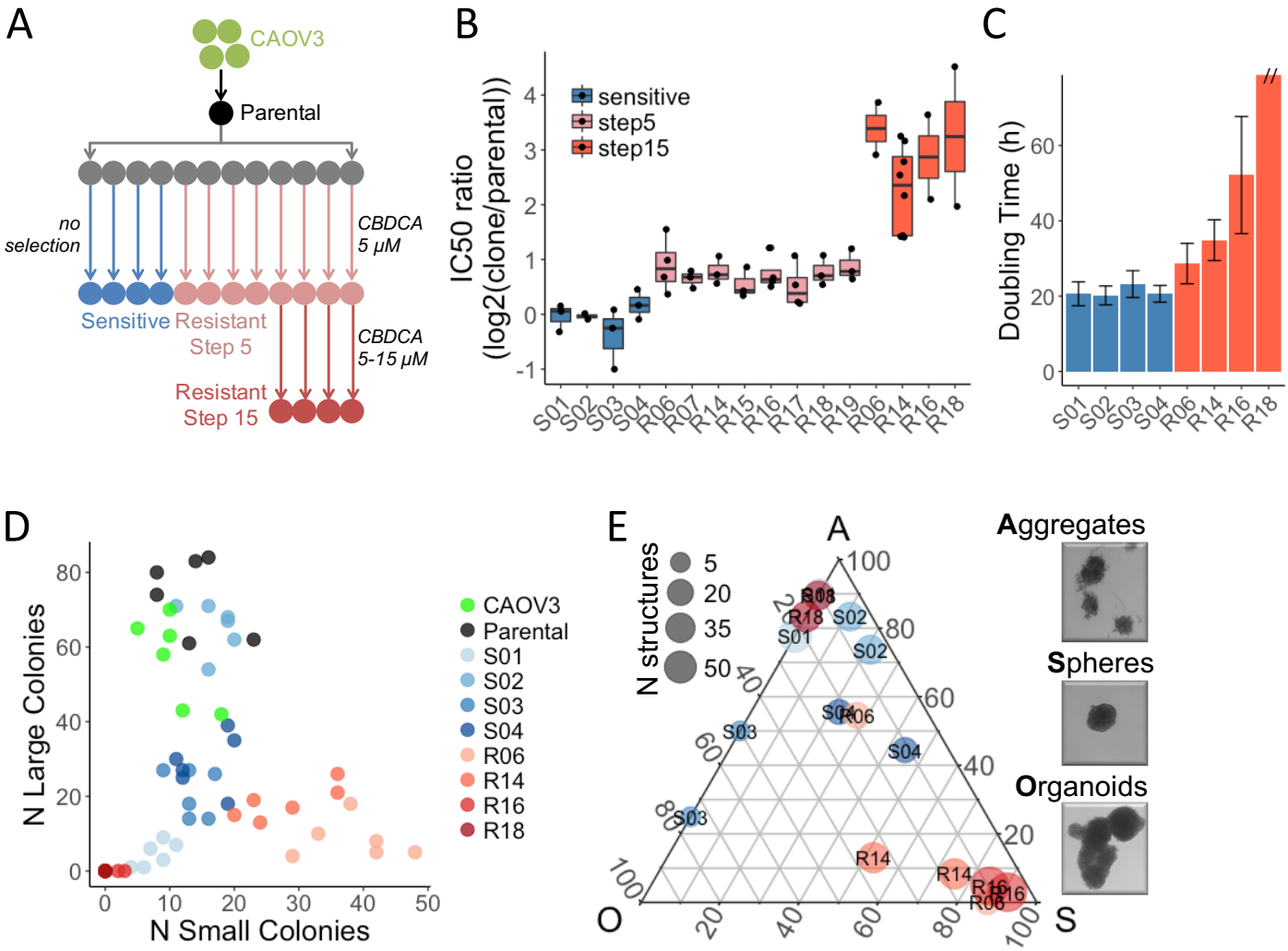

Figure 1: Phenotypic characterization of the resistant clones. (A) Schematic representation of the workflow to generate CBDCA resistant clones from CAOV3. **(B)** Changes in IC50 of S clones (unselected) or R clones (8 at step 5 and 4 at step 15). Each IC50 is calculated from dose-response curves of 6 replicates and experiments repeated twice or more (dots). **(C)** Doubling time measured over a 48 h time course – y axis cut for R18 (>100 h). **(D)** Counting of colonies formed in a period of 9 days after seeding 200 cells per well. Experimental replicates (N=6) are shown. **(E)** Fraction of organoids (O), spheres (S) and cell aggregates (A) observed after 14 days growth in low adherence 3D culture model. For each sample (N=8) and replicates (N=2), the total number (point size) and relative abundance (Gibbs triangle coordinates) of each type of structure are indicated.

bioRxiv preprint doi: https://doi.org/10.1101/231548; this version posted December 8, 2017. The copyright holder for this preprint (which was not certified by peer review) is the author/funder, who has granted bioRxiv a license to display the preprint in perpetuity. It is made available under aCC-BY-NC-ND 4.0 International license.

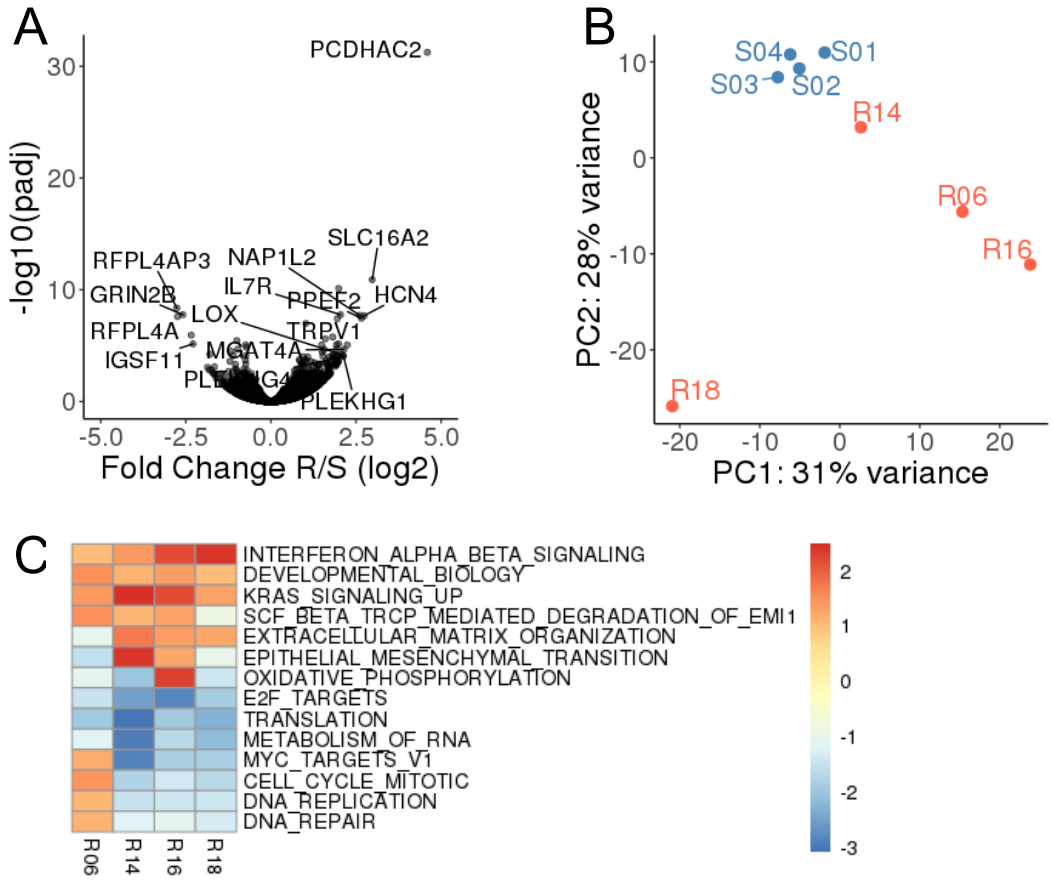

Figure 2: Expression profiling of the derived clones. (A) Volcano plot indicating the fold change (y axis) and significance (x axis) of the genes differentially expressed between S and R clones. **(B)** First two principal components derived from the expression profiles of each clone. **(C)** Most significantly up or down-regulated gene sets (Hallmark and Reactome) in individual R clones compared to all S clones. Significant gene sets (q.value<0.005) enriched (score>1.5) or depleted (score <-2) in at least one clone are reported. Color gradient indicates enrichment score.

bioRxiv preprint doi: https://doi.org/10.1101/231548; this version posted December 8, 2017. The copyright holder for this preprint (which was not certified by peer review) is the author/funder, who has granted bioRxiv a license to display the preprint in perpetuity. It is made available under aCC-BY-NC-ND 4.0 International license.

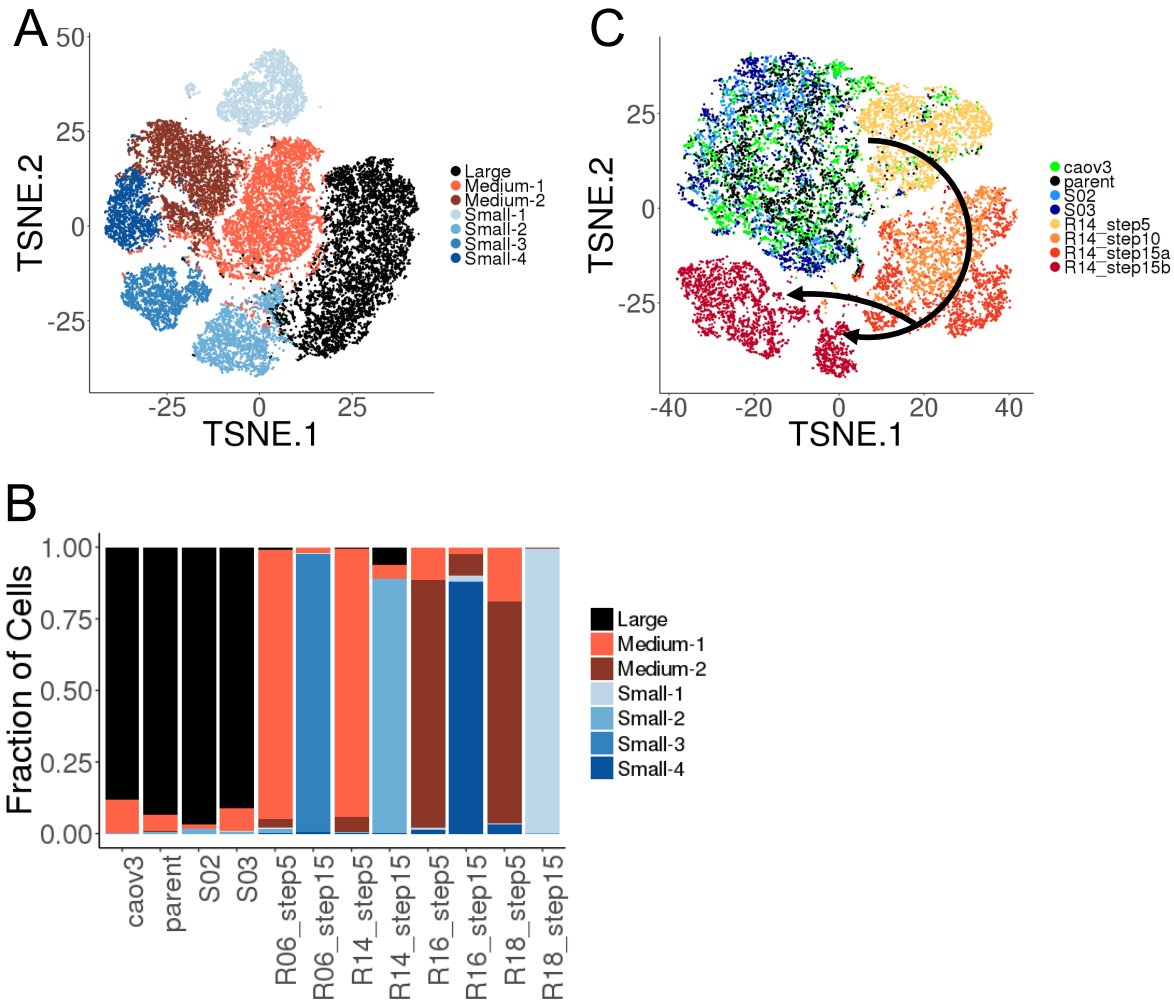

Figure 3: Identification of single cell resistant states. (A) tSNE projection of 28,982 single cells from CAOV3, parental clone, S02, S03 as well as four R clones (after step 5 and step 15 selection). Cell are colored according to the 7 clusters identified. **(B)** Proportion of cells located in each cluster. **(C)** tSNE projection of 17,320 single cells from CAOV3, parental clone, S02, S03 as well as four R14 selection steps: step 5, step 10, step 15a (40 drug-free doublings) and step 15b (77 drug-free doublings). The arrows highlight the transition between states during the progression of the selection.

bioRxiv preprint doi: https://doi.org/10.1101/231548; this version posted December 8, 2017. The copyright holder for this preprint (which was not certified by peer review) is the author/funder, who has granted bioRxiv a license to display the preprint in perpetuity. It is made available under aCC-BY-NC-ND 4.0 International license.

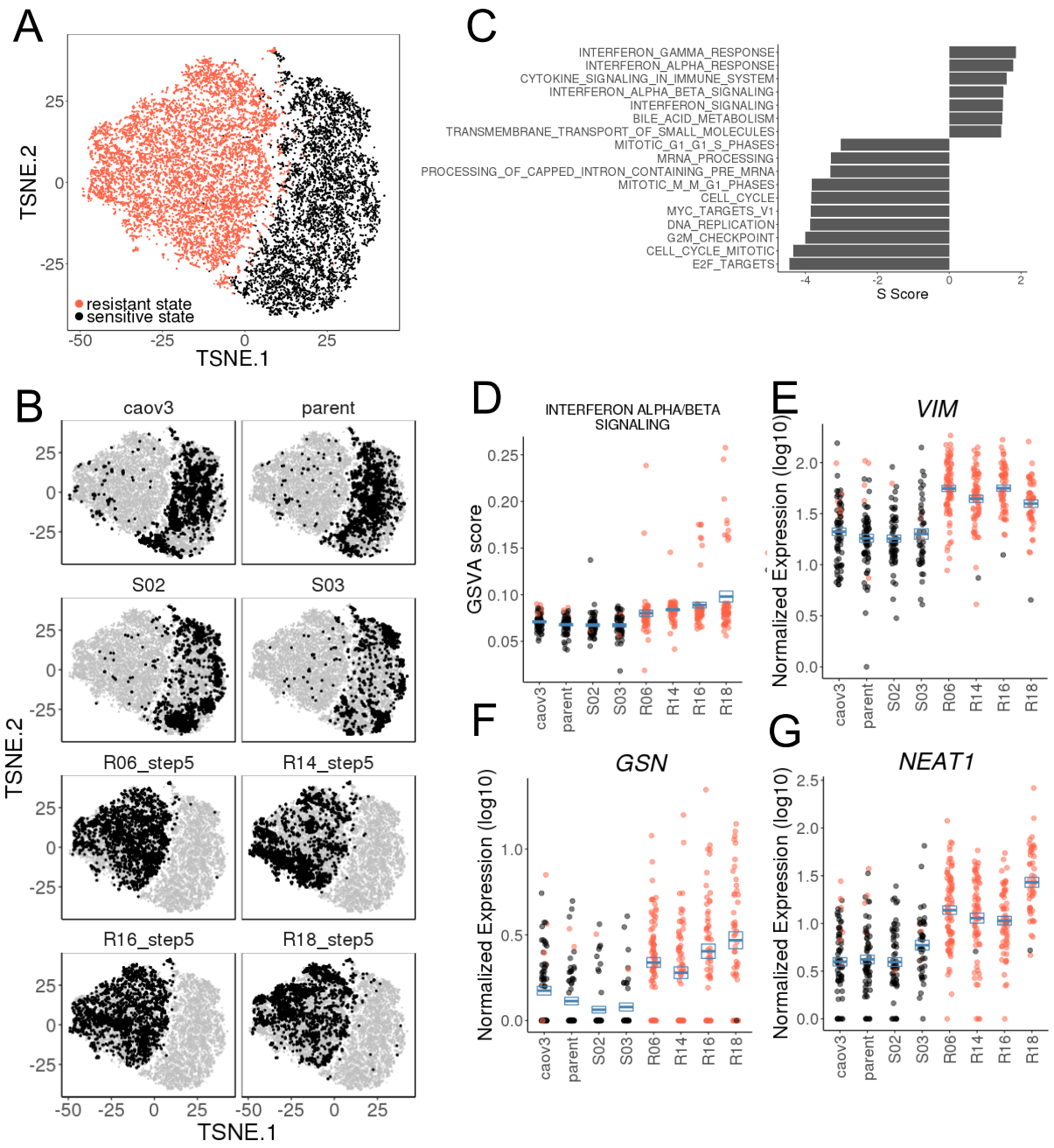

Figure 4: Single cell expression analysis after step 5 selection. (A) tSNE projection of 17,230 single cells from 8 samples (COAV3, parental, S02, S03, R06, R14, R16, R18). The two main clusters corresponding to sensitive (black) and resistant (red) states are indicated. **(B)** tSNE projection identical to (A) and highlighting the location of cells from each sample in their respective panel (black). **(C)** Most significantly up or down-regulated processes (Hallmarks and Reactome) in cells located in the resistant state (q.value<0.01). All Hallmark (N=50) and Reactome (N=674) gene sets were included in the analysis. **(D-G)** Single cell (N=500) interferon signaling score (D) or expression level for Vimentin (E), Gelsolin (F) or *NEAT1* non-coding RNA (G). The state of each cell is indicated (red: resistant, black: sensitive). The blue boxes represent mean and standard error.

bioRxiv preprint doi: https://doi.org/10.1101/231548; this version posted December 8, 2017. The copyright holder for this preprint (which was not certified by peer review) is the author/funder, who has granted bioRxiv a license to display the preprint in perpetuity. It is made available under aCC-BY-NC-ND 4.0 International license.

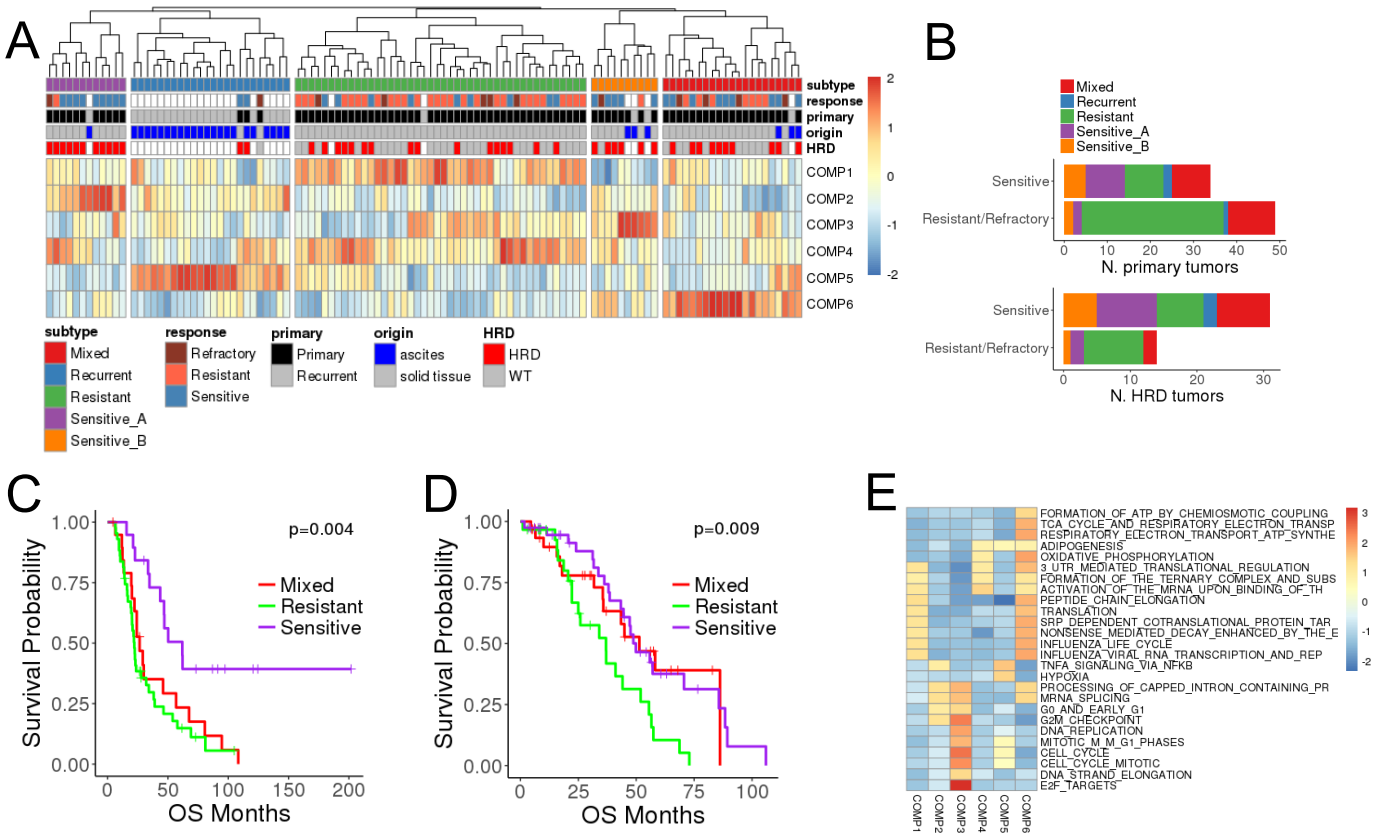

Figure 5: Resistance-based patient stratification. (A) NMF-based classification of 111 high grade serous ovarian cancer from Patch et al. (20). The level of the 6 transcriptional components are indicated in heatmap scale, the 5 resulting subtypes are color coded. **(B)** Distribution of all (upper panel) or HRD (lower panel) primary tumors across subtypes (colors) and primary response (y – axis). **(C)** Kaplan-Meier plot of overall survival (OS) of ICGC primary tumors from the three major states (Sensitive=Sensitive A+Sensitive B). The log rank test p-value is indicated. **(D)** same as (C) for TCGA tumors. 101/270 TCGA primary tumors were robustly assigned to a subtype (maximum Pearson correlation > 0.2). **(E)** Reactome pathway Gene set enrichment scores (heatmap) in each NMF component. The most significantly enriched gene sets (p<3 x10-3) in at least one component are represented.

bioRxiv preprint doi: https://doi.org/10.1101/231548; this version posted December 8, 2017. The copyright holder for this preprint (which was not certified by peer review) is the author/funder, who has granted bioRxiv a license to display the preprint in perpetuity. It is made available under aCC-BY-NC-ND 4.0 International license.

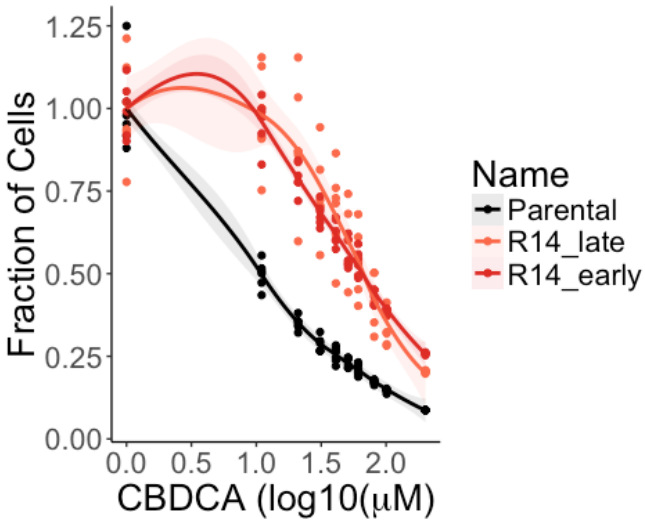

Figure S1: Dose Response comparing the drug sensitivity of R14 clones after 36 (R14_early) and 99 (R14_late) doublings after step 15 selection.

bioRxiv preprint doi: https://doi.org/10.1101/231548; this version posted December 8, 2017. The copyright holder for this preprint (which was not certified by peer review) is the author/funder, who has granted bioRxiv a license to display the preprint in perpetuity. It is made available under aCC-BY-NC-ND 4.0 International license.

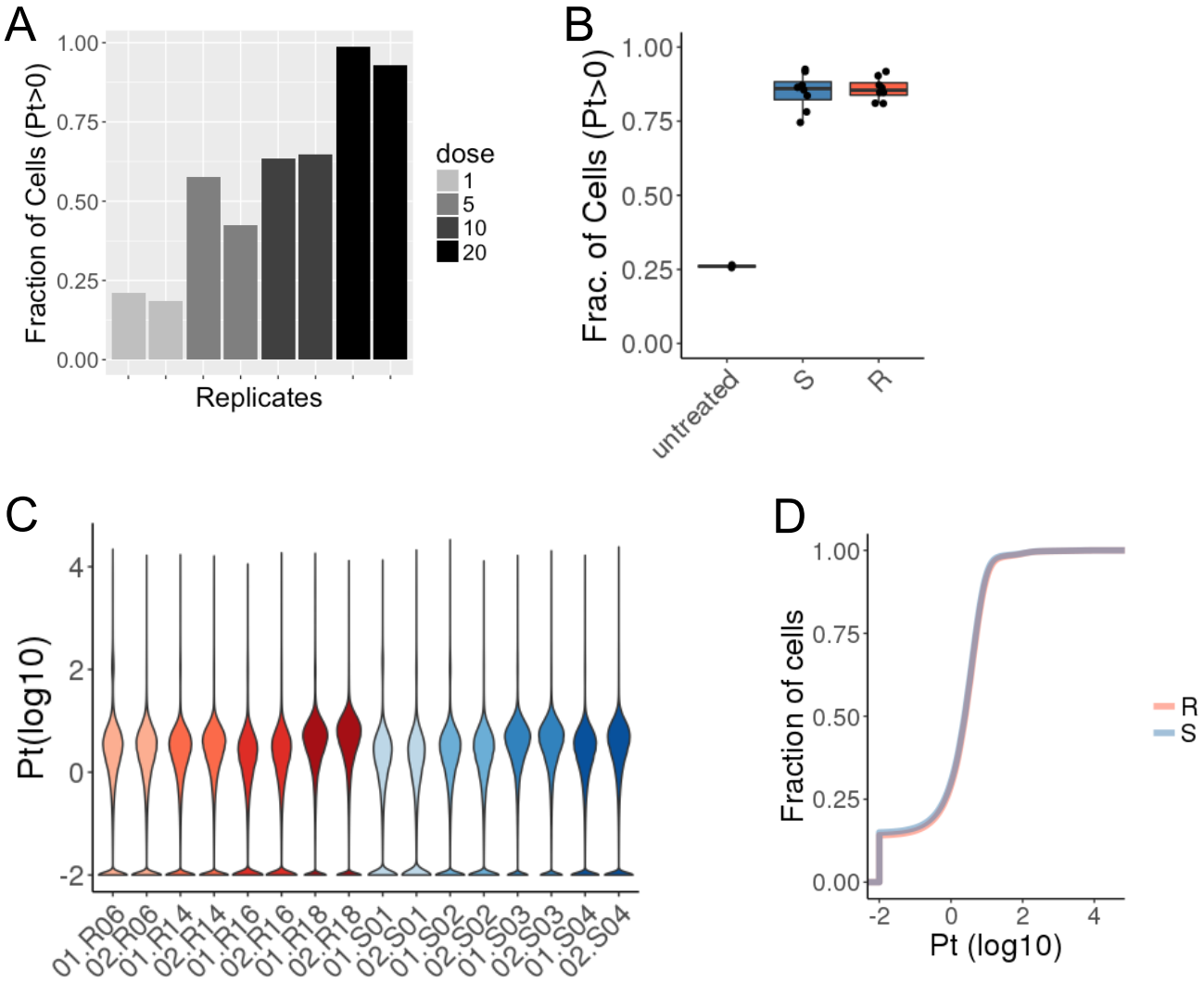

Figure S2: Pt uptake measured by mass cytometry. (A) The fraction of cells with detectable Pt content was measured after 1 h treatment with increasing dose of carboplatin (x axis, grey color gradient). **(B)** Fraction of cells with detectable levels of Pt. Each clone and replicate are represented. **(C)** Violin plot showing the distribution of Pt content across cells from all clones and replicates. **(D)** Cumulative distribution of Pt content between cells from R and S clones and replicates. The Pt negative cells were assigned at 0.01 Pt content for graphical representation (C and D).

bioRxiv preprint doi: https://doi.org/10.1101/231548; this version posted December 8, 2017. The copyright holder for this preprint (which was not certified by peer review) is the author/funder, who has granted bioRxiv a license to display the preprint in perpetuity. It is made available under aCC-BY-NC-ND 4.0 International license.

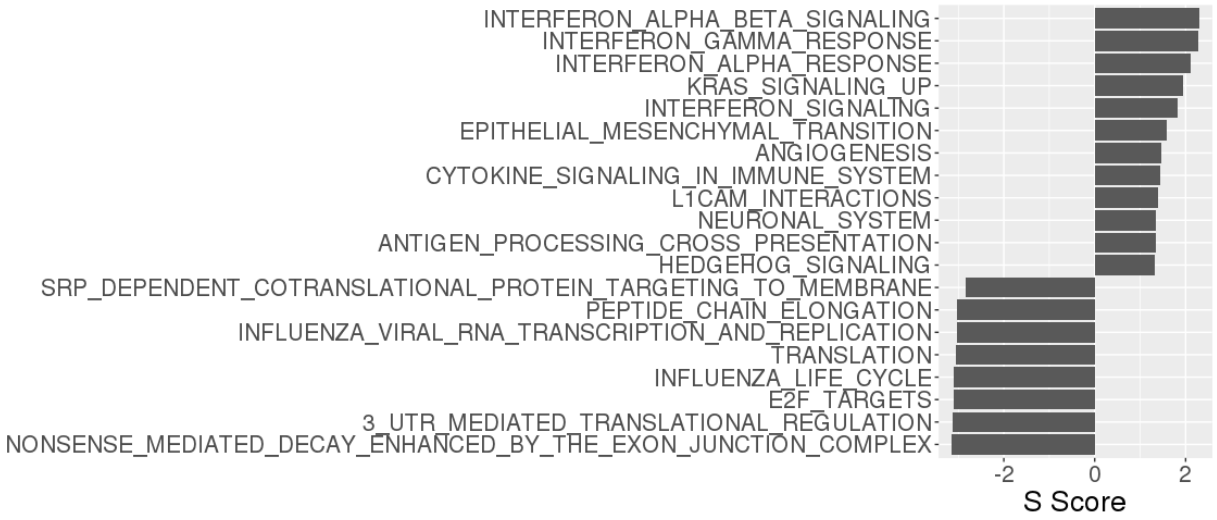

Figure S3: Most affected pathways in the resistant clones. Most significantly up or down-regulated processes in CBDCA resistant clones after step 15 selection (q.value<0.05). All Hallmark (N=50) and Reactome (N=674) gene sets were included in the analysis.

bioRxiv preprint doi: https://doi.org/10.1101/231548; this version posted December 8, 2017. The copyright holder for this preprint (which was not certified by peer review) is the author/funder, who has granted bioRxiv a license to display the preprint in perpetuity. It is made available under aCC-BY-NC-ND 4.0 International license.

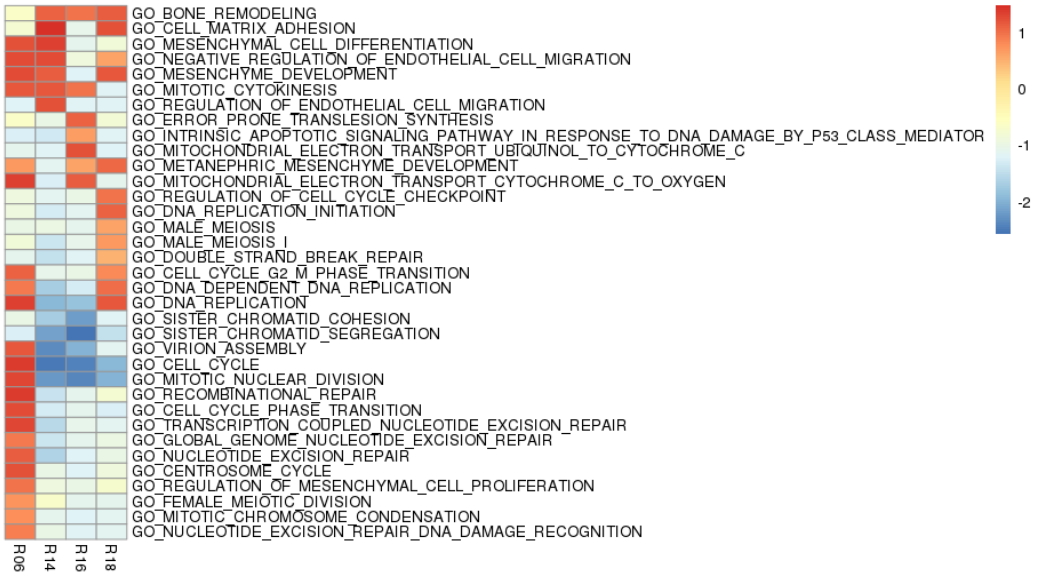

Figure S4. Most significantly altered clone-specific GO biological processes. The enrichment of gene sets from GO biological processes (N=136 from DNA repair and cell cycle related GO) was determined and the most significant (q.val<0.05) and most clone specific (standard deviation >0.5) are reported.